Available online at www.sciencedirect.com
SCIENCE DIRECT
Journal of Sound and Vibration 295 (2006) 165–193
JOURNAL OF SOUND AND VIBRATION
www.elsevier.com/locate/jsvi

Estimation of complex modulus using wave coefficients

Yabin Liao*, Valana Wells

Department of Mechanical and Aerospace Engineering, Arizona State University, P.O. Box 876106, Tempe, AZ 85287-6106, USA

Received 16 June 2005; received in revised form 8 December 2005; accepted 30 December 2005
Available online 10 March 2006

Abstract

The paper presents a new, efficient and accurate method for experimentally determining structural damping properties of stiff materials in flexural vibration. The estimation method seeks a wavenumber that forces data at all measurement points to conform with the general forced-vibration solution for a beam, and, thus, to have the same wave coefficients. The method does not depend on beam boundary conditions, making it relatively simple to implement in any laboratory setting. The paper shows results of using the method to estimate the complex modulus of aluminum and of polymethyl methacrylate (PMMA) beams in the frequency range from 30 to 800 Hz.Results compare very well with those obtained by more conventional methods and with those previously published over most of the frequencies of interest. Discrepancies in results for frequencies less than 80 Hz are attributed to the difficulty in measuring differences of velocity between points that are near each other at low frequency, and a technique for avoiding such discrepancies is outlined. Evidence shows that the error in the results near 350 Hz is due to a resonance in the scanning laser vibrometer that was used to take the experimental measurements.

1. Introduction

Correct prediction of system dynamic behavior and efficient use of damping material in a design require accurate knowledge of viscoelastic material properties. Since the 1950s, many methods have been developed for measuring a material's complex modulus of elasticity (also called Young's modulus). Many of these experimental techniques have utilized beam configurations. Advantages of beam methods include the fact that beam theory is well developed and understood and that experimental setup is straightforward. An additional advantage of using beams arises because material damping may depend not only on the material itself, but also on the configuration and conditions under which it is utilized. It is thus recommended that any test should bear a close resemblance to the final application [1]. Since damping of plates has been of the most interest in practice, and since bending waves are the most important type of vibration waves to control [2], it is appropriate to perform experiments that measure the complex modulus arising from bending waves on beams, which are simply special cases of plates in one dimension.

Conventional vibrating-beam techniques can be roughly grouped into two categories: 1) methods that exploit the intrinsic eigen-structure (modal structure) of the beams [1–3], and (2) methods based on the

*Corresponding author. Tel.: +1 480 965 8107; fax: +1 480 965 1384.
E-mail address: yabin.liao@asu.edu (Y. Liao).

0022-460X/$ - see front matter © 2006 Elsevier Ltd. All rights reserved.
doi:10.1016/j.jsv.2005.12.045

propagating wave model [2,4]. For materials not stiff enough to be measured directly, material layers can be applied to a base beam and then layer theories [2,3,5,6] can be used to extract their properties from the effective complex modulus of the layer system. (These materials are not addressed in the current work.) However, there are two disadvantages or restrictions associated with these methods: first, for group 1 methods, the complex modulus can only be evaluated at resonance frequencies, and the damping must be small to obtain accurate results; second, most of the methods depend on specific boundary conditions that might not be easy to achieve in reality, especially for methods in group 2.

The search for an experimental technique that accurately and easily measures material damping has been ongoing. Hull and Hurdis [7] derived a closed form solution for the wave number from seven transfer functions measured at evenly spaced locations. They showed that, although the wavenumber could be determined exactly using five measurements, more accuracy in estimating was achieved by using seven measurements. The wave coefficients can then be determined exactly, or estimated using least-squares algorithm, the latter being preferred because it is more robust. Recently, Hillström, Mossberg and Lundberg proposed a complex modulus estimation method using least squares [8–11] that can be applied to data sets comprised of unevenly spaced measurement locations. Both of the above approaches have advantages that the complex modulus can be measured continuously in a wide frequency range not restricted to resonance frequencies, and the method does not depend on boundary conditions. Concurrently, McDaniel and Shepard [12] described a method very similar to that of Hillström et al.

This paper presents a complex-modulus-estimation algorithm, termed the Wave Coefficients Method (COE), which is related to the above approaches in the 'optimization' sense but was developed independently using a different philosophical basis. The following narrative introduces the mathematical foundation for the new algorithm and its differences from Hillström et al.'s Least-Squares (LS) method. Results from experiments on an aluminum beam and a PMMA beam in the frequency range between 30 and 800 Hz and obtained using the COE and the LS methods, are presented and compared with those obtained by using several conventional vibrating-beam techniques.

The governing equation of motion for the transverse vibration of a uniform beam in phasor form is

$$EI\frac{\partial^4 \hat{y}}{\partial x^4} - \rho A\omega^2 \hat{y} = 0, \tag{1}$$

where $\hat{y}$ is the transverse displacement of the beam (the actual physical displacement in time domain, $y(x,t)$ is the real part of $\hat{y}(x,\omega)e^{i\omega t}$), E is Young's modulus, I is the second moment of area, ρ is the beam density, and A is the cross-sectional area. E and $\hat{y}$ may be complex-valued while the other parameters are real. Conventionally, the complex modulus can be expressed as $E = E'(1 + i\eta)$, where E' is the real modulus and η is the loss factor. In deriving Eq. (1), the effects of both the shear deformation and the rotatory inertia are neglected. For beams that are long compared to their cross-sectional dimensions, these effects are small [2].

From Eq. (1) the steady-state vibration velocity at location x on the beam can be expressed as

$$\hat{v} = ae^{-ikx} + be^{ikx} + ce^{-kx} + de^{kx}, \tag{2}$$

where k is the complex wavenumber, which can be calculated as

$$k = \sqrt[1/4]{\frac{\omega^2 \rho A}{EI}} \tag{3}$$

and a, b, c, and d are called propagating wave coefficients, which can be determined from boundary conditions. The ae^{-ikx} solution term can be interpreted as a wave propagating along the positive x axis, and the be^{ikx} term, a wave propagating along the negative x-axis. ce^{-kx} and de^{kx} are near-field terms. ω is the angular frequency, which is real-valued.

Eq. (3) can be rearranged to give

$$E = \frac{\omega^2 \rho A}{k^4 I}, \tag{4}$$

which relates the complex modulus to complex wavenumbers. Therefore, the problem becomes one of measuring the wavenumbers in order to calculate the real and imaginary parts of the complex modulus.

The method to identify the wavenumber k in Eq. (2) is presented in the next section. Given the identified k, E can be calculated using Eq. (4) by noting that ω, I, ρ, and A are parameters that are measurable or controllable.

2. The wave coefficients method

The wave coefficients algorithm (COE method) is based on the simple concept that the steady-state motions of all points on a uniform beam must satisfy Eq. (2), i.e., they should have the same wave coefficients a, b, c and d for any given frequency (or wavenumber).

Say N measurements of the vibration velocity, $\hat{v}_1$, $\hat{v}_2 \ldots \hat{v}_N$, are available at locations x_1, $x_2 \ldots x_N$. There are 5 unknowns in Eq. (2), four wave coefficients and one wavenumber. Mathematically this requires that N should be equal to or larger than 5 to determine or over-determine the system unknowns.

A system of equations can be formed from any 4 of the measurements:

$$\mathbf{v}_p = \mathbf{M}_p \mathbf{w}_p, \tag{5}$$

where

$$\mathbf{v}_p = \begin{bmatrix} \hat{v}_i \\ \hat{v}_j \\ \hat{v}_l \\ \hat{v}_m \end{bmatrix}, \quad \mathbf{M}_p = \begin{bmatrix} e^{-ikx_i} & e^{ikx_i} & e^{-kx_i} & e^{kx_i} \\ e^{-ikx_j} & e^{ikx_j} & e^{-kx_j} & e^{kx_j} \\ e^{-ikx_l} & e^{ikx_l} & e^{-kx_l} & e^{kx_l} \\ e^{-ikx_m} & e^{ikx_m} & e^{-kx_m} & e^{kx_m} \end{bmatrix}, \quad \mathbf{w}_p = \begin{bmatrix} a_p \\ b_p \\ c_p \\ d_p \end{bmatrix}. \tag{6}$$

i, j, l and m are measurement point indices in the range of 1 to N, and p is the combination index which starts from 1 to $\binom{N}{4}$ since there are a total of $Q = \binom{N}{4}$ ways to select 4 measurement points out of N measurement points.

A set of wave coefficients can be calculated for each combination by assuming a tentative wavenumber in $\mathbf{M}_p$:

$$\mathbf{w}_p = \mathbf{M}_p^{-1} \mathbf{v}_p, \tag{7}$$

where $p = 1,2,\ldots,Q$.

Then an error function is calculated as

$$e(k) = \frac{\sqrt{var(a_1, a_2, \ldots, a_Q)}}{|\text{mean}(a_1, a_2, \ldots, a_Q)|} + \frac{\sqrt{\text{var}(b_1, b_2, \ldots, b_Q)}}{|\text{mean}(b_1, b_2, \ldots, b_Q)|}, \tag{8}$$

which is a function of the trial wavenumber.

Theoretically this error function should be zero at the *real wavenumber* since all of the points on the beam should have the same wave coefficients. Based on this fact, the procedure of the wavenumber identification algorithm can be summarized as following: (1) assume a tentative wavenumber; (2) compute all the wave coefficients for the assumed wavenumber; (3) compute the error function; (4) repeat 1–3 until a wavenumber that minimizes the error function is found.

In this study, the core identification process is handled by the FMINSEARCH function of Matlab. The FMINSEARCH function starts at an initial guess for the wavenumber, and automatically varies the real and imaginary parts of the wavenumber until it finds a local minimizer of the defined error function, i.e., the COE error as defined in Eq. (8).

The error function does not include the wave coefficients c and d because they are associated with near-field terms, which are significant only near boundaries. As will be shown in Section 7.2.1, the ae^{-ikx} and be^{ikx} are dominant wave terms in the overall wave field at most of frequencies of interest. Therefore, in some sense the wave coefficients a and b are parameters associated with high signal-to-noise ratio measurements, while c and d are related to low signal-to-noise measurements. Numerical error analysis in Section 7.2.1 will show that including the coefficients c and d in the error function actually degrades the estimation performance.

3. The least-squares estimation method

The LS estimation method [8] follows a procedure that is, in some ways, similar to that of the COE method: (1) assume a tentative wavenumber; (2) use the classic least-squares algorithm to find an 'optimized' set of wave coefficients for this tentative wave-number; (3) reconstruct a wave field using the tentative wavenumber and the 'optimized' set of wave coefficients; (4) compute the error function, which is defined as the difference between the measured wave field and the reconstructed wave field; (5) repeat 1–4 until a wave number that minimizes the error function is found.

There is, however, a major underlying difference between the two concepts: the LS method finds a wavenumber that generates a vibration wave field best approximating the measurements, while the COE method seeks a wavenumber that forces the measurement points to have, as close as possible, the same wave coefficients.

4. Experimental setup

The experimental setup is shown in Fig. 1. One end of the test beam is free while the other end is clamped to a shaker (MB Dynamics PM50A), which provides the excitation to the beam. The excitation source signal comes from a function generator (Hewlett Packard 33120A), then is augmented by an amplifier (MB Dynamics SS250). A scanning laser Doppler vibrometer system (Polytec PSV-200) is used to measure the vibration velocity wave field of the beam. The non-contacting scanning laser Doppler vibrometer can provide accurate vibration velocity measurements, and it has the advantage that, unlike accelerometers or strain gauges mounted on the apparatus, it provides non-intrusive measurements. To obtain the phase information

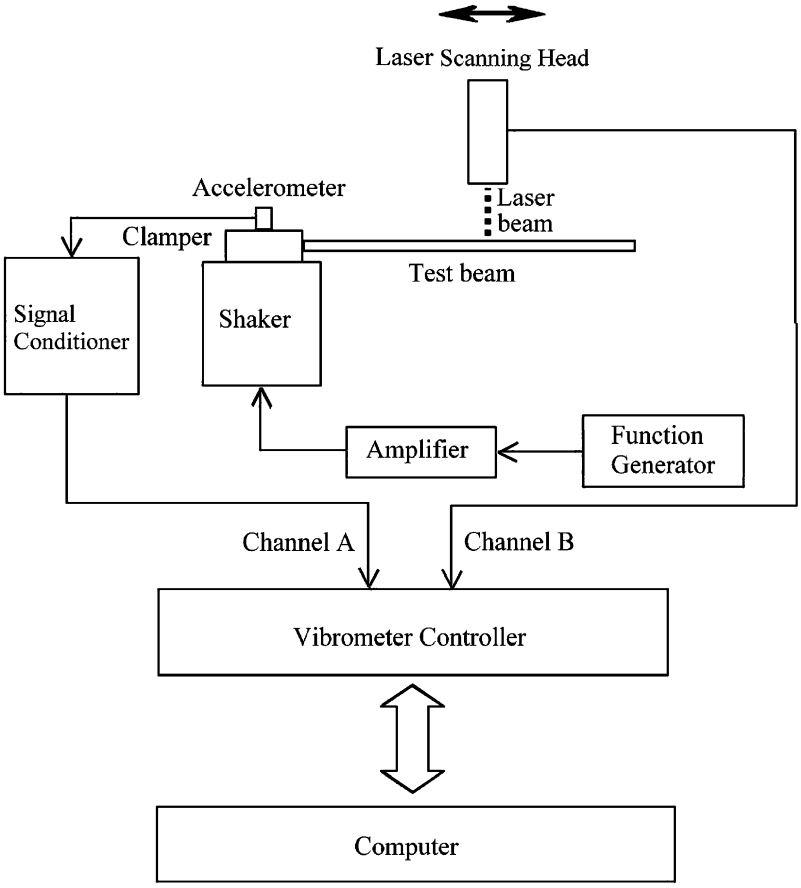

Fig. 1. Experimental setup.

for the wave field, an accelerometer (PCB Piezotronics 353B17) is placed on the clamp to provide a reference signal. The acceleration signal first goes through a signal conditioner (PCB Piezotronics 482A16) and then is picked up by the vibrometer controller as Channel A signal. The Channel B of the controller is set by default as the vibration velocity signal. A PC directs the vibrometer controller and performs the data acquisition and processing. The two channel signals are first conditioned by the controller according to the data acquisition settings and then converted to the PC through an A/D board. PSV-200 software is used for data acquisition. The PSV software has the capability to easily compute transfer functions, and, in fact, it is the transfer function between the output beam velocity and the input shaker velocity, rather than the beam velocity itself, that was utilized in the calculations in this work. Matlab is used to execute the LS and COE algorithms to estimate the complex modulus.

5. Aluminum beam experimental results

The complex modulus estimation methods were first applied on a nearly undamped material, aluminum, which has a negligible loss factor of order 10^{-4} [2].

A rectangular-cross-section aluminum (CA 6061-T6511) beam was tested at temperatures near 23.0 °C. The beam was clamped at one end to the shaker and was free at the other end. The beam had a cantilever length of 279 mm. Its thickness was 3.14 mm, its width was 19.05 mm, and its density was 2709 kg/m^3.

The excitation was sinusoidal. Before any measurements were taken, the vibration velocity field was checked to make sure that steady state had been reached for the test system. A typical waiting time was 30 min.

The maximum amplitude of the vibration velocity of the test beam was controlled to be close to but lower than 50 mm/s. The vibrometer had a velocity measurement resolution of 3 μm/s. The sampling frequency was 5120 Hz and the frequency resolution was 0.625 Hz. Two different measurement-point combination sets were used for each frequency; and each combination had 7–9 measurement points. For example, for the frequency 250 Hz, one set of measurement points was at positions [0.03, 0.09, 0.12, 0.15, 0.18, 0.23, 0.26] m starting from the clamp end (whose position was 0.00 m); and the other set was at [0.02, 0.08, 0.11, 0.14, 0.17, 0.20, 0.25] m.

The experimental results of the tests for the aluminum beam using the (COE) and the LS methods are shown in Fig. 2.

Fig. 2 shows that the COE method and the LS method yield very similar results. The real modulus for the aluminum beam first increases as frequency increases, reaches its maximum of about 70 GPa at a frequency between 300 and 400 Hz and then decreases. Within the test frequency range, the average real modulus of the test beam is approximately 65.5 GPa. A typical real modulus value for 6061-T6511 aluminum beam is 68.9 GPa [13]. Fig. 2 also shows that most of the estimated loss factors for the aluminum beam fall between $\pm$ 0.015, and this is in agreement with the fact that aluminum is a very low damping material. However, at 350 Hz the estimated loss factor is -0.07, which is far below those at other frequencies. The cause of the poor performance of the methods at this frequency will be discussed in Section 7.2.

A numerical error analysis determined an estimate of the error in these results. The analysis proceeded as follows: first the LS method was used to identify the complex wavenumber from the experimental measurements at a specific frequency. Then the corresponding 'optimized' wave coefficients were obtained for this complex wavenumber. Since aluminum is virtually damping-free, the imaginary part of the wavenumber was discarded. The identified wavenumber and the 'optimized' wave coefficients were used to construct a new known wave field. As shown in Fig. 3, the simulated vibration nearly exactly matches the measured field, as expected. Then random Gaussian noise was added to the wave field. The noise was added to the magnitude and phase angle of the vibration velocity, and measurement position as well. Table 1 shows the statistics of the added Gaussian noise, which was chosen to be a slightly larger than, but of the same order of magnitude, as the actual experimental noise. Finally, the LS and the COE methods were applied to the simulated, noisy data in order to estimate the modulus.

The process was repeated 500 times for each experimental wave field measurement. The statistics of the results are presented in Fig. 4, where $e_{E'}$ is the normalized real modulus estimation error defined as

$$e_{E'} = \sqrt{\frac{1}{L}\sum_{r=1}^{R}\left(\frac{E'_{\mathrm{Est}}}{E'_{\mathrm{Sim}}} - 1\right)^2}, \tag{9}$$

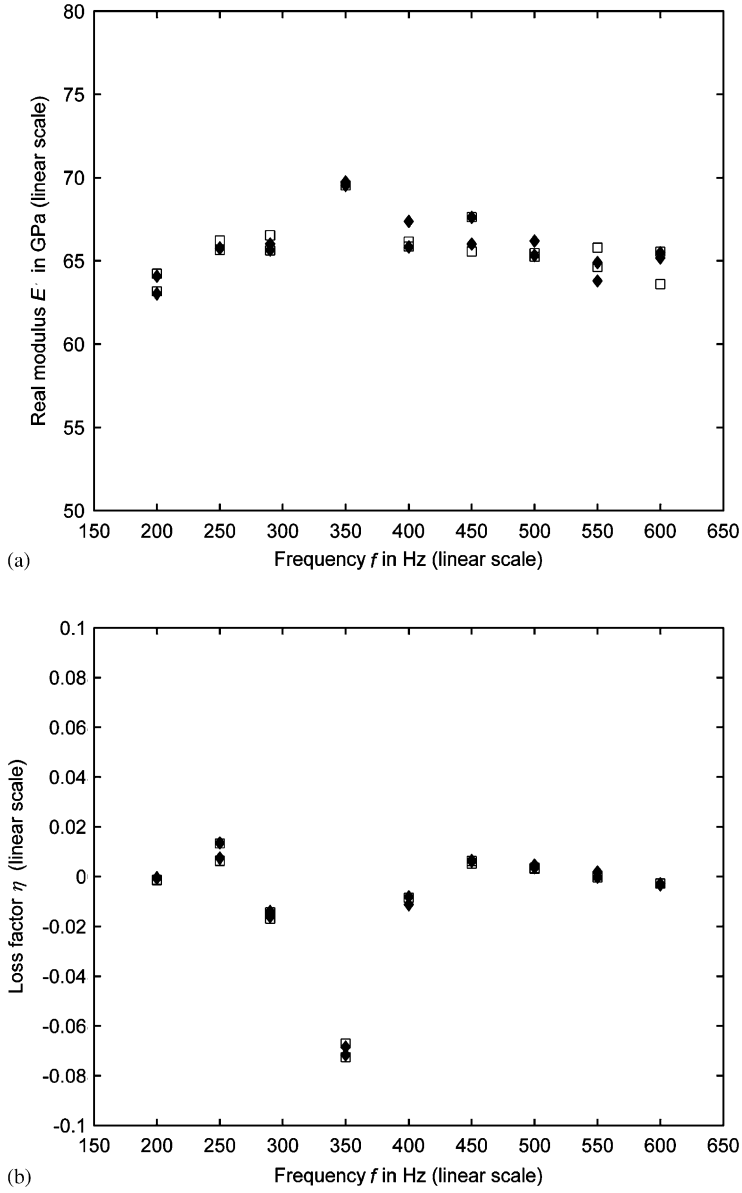

Fig. 2. Complex modulus E vs. frequency f for aluminum. (a) Real modulus E'; (b) loss factor η. ◆, Wave coefficients (COE) method results; □, Least-Squares (LS) method results.

with E'_{Sim} being the real modulus used to simulate the noise-free wave field measurement, and E'_{Est} the real modulus estimated by the methods from the noise-added measurement. The quantity, e_η represents the loss factor estimation error defined as

$$e_\eta = \sqrt{\frac{1}{R}\sum_{r=1}^{R}(\eta_{\mathrm{Est}} - 0.00)^2}, \tag{10}$$

where η_{Est} is the loss factor estimated from the noise-added measurement. The total number of Monte-Carlo simulations, R, is 500. The number "0.00" in the equation is written out explicitly to emphasize that the (simulated) loss factor for the noise-free wave fields is zero.

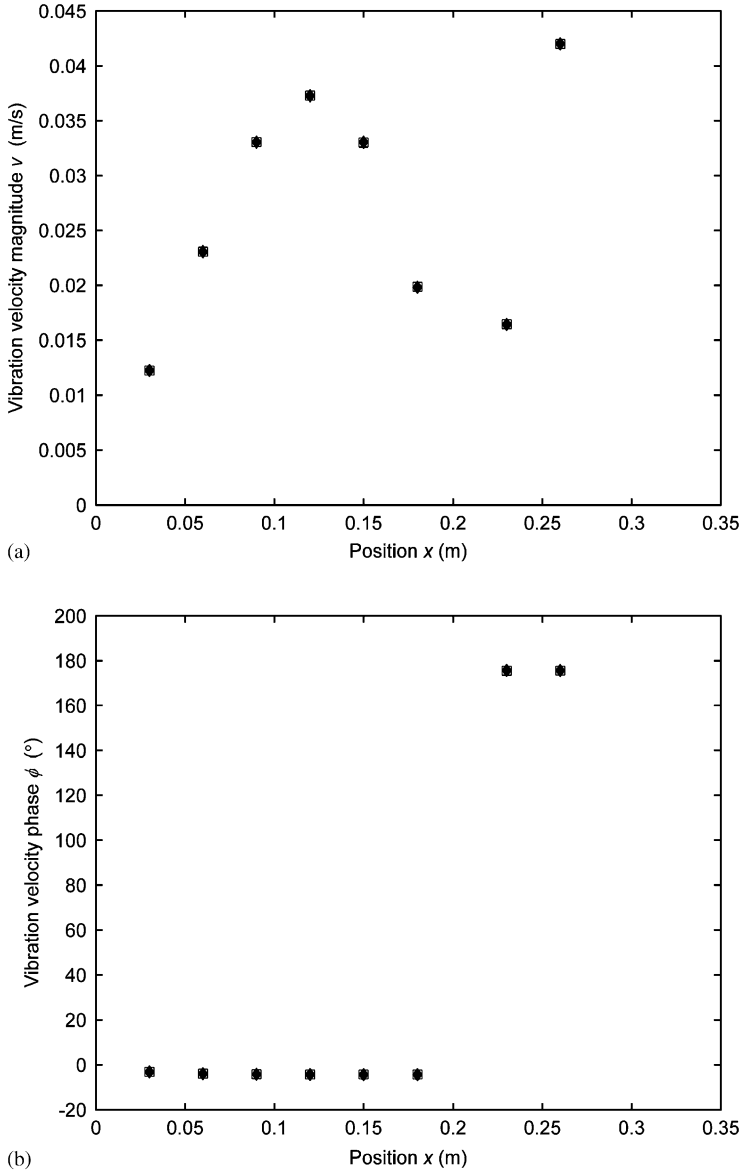

Fig. 3. Comparison of Measured and Simulated vibration velocities on the aluminum beam. (a) Vibration velocity magnitude; (b) vibration velocity phase. ◆, experimental measurements; □, simulated results.

Table 1
Added Gaussian noise statistics

Noise type	Standard deviation
Position	0.15 mm
Magnitude	0.15 mm/s
Phase angle	0.25°

Fig. 4 shows that the normalized real modulus estimation error $e_{E'}$ is below 0.04 (or 4 percent in percentage error sense) at all simulation frequencies. The loss factor estimation error e_η is about 0.015 for most of the frequencies. Statistically speaking, assuming that the estimation results are Gaussian-distributed,

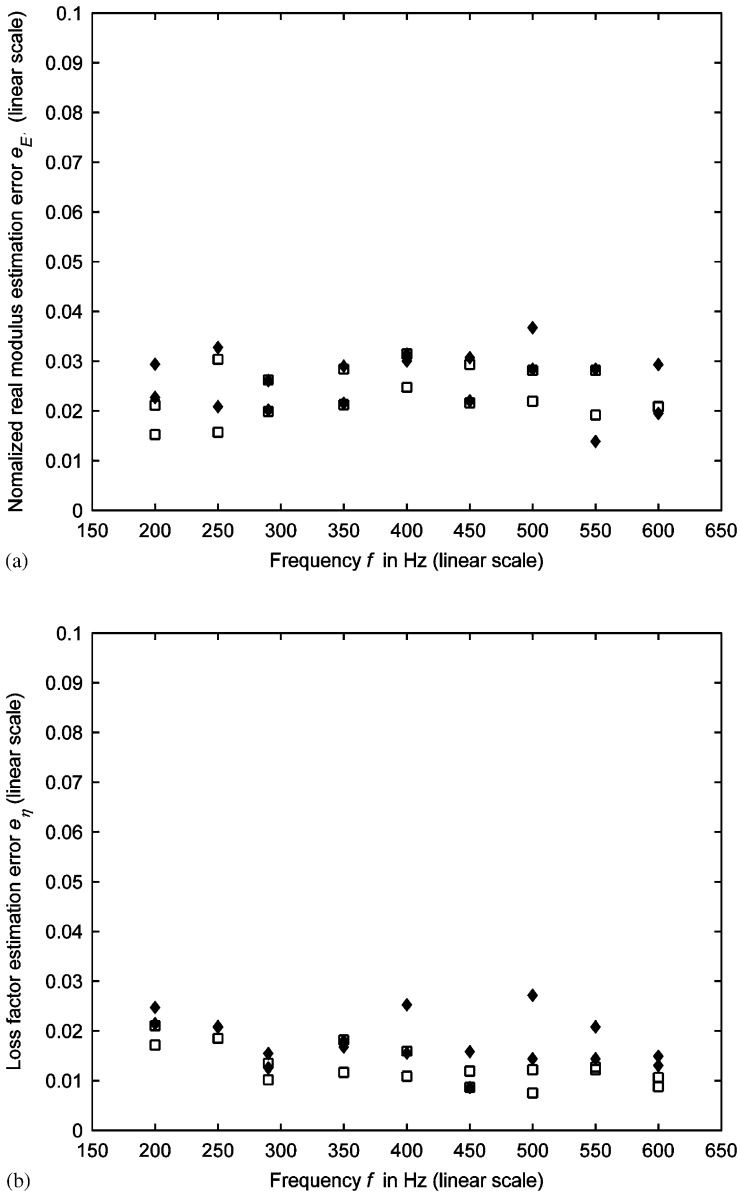

Fig. 4. Complex modulus estimation error vs. frequency f for estimating simulations of the aluminum beam. (a) Normalized real modulus estimation error $e_{E'}$; (b) loss factor estimation error e_η. ◆, Wave coefficients (COE) method; □, Least-Squares (LS) method.

approximately 68% of the estimated loss factors fall into the range ± 0.015. This is in agreement with the experimental results as shown in Fig. 2.

For the error analysis, two different combinations of measurement points were used for each frequency. Fig. 4 shows that at several frequencies one combination is associated with noticeably less error than the other, for example, at 400, 500 and 550 Hz. The error analysis can help in choosing point combinations that are more robust with respect to experimental noise and, consequently, in obtaining more accurate results. Another way to improve the performances of the methods is to increase the total number of measurement points, or to increase the distance between measurement points, or both. This will be demonstrated in Section 7.2.

6. PMMA experimental results

A rectangular cross-section PMMA beam was tested at temperatures near 22.5 °C. The test beam was clamped at one end and free at the other with a cantilever length of 340 mm. It had thickness 4.42 mm and width 20 mm. The density was 1183.6 kg/m^3. The shaker produced sinusoidal excitation at frequencies between 30 and 800 Hz. The system reached steady state after a waiting time of approximately 20 min. The maximum amplitude of the vibration velocity of the test beam was controlled to be close to but lower than 50 mm/s. The velocity measurement resolution of the vibrometer was 3 μm/s. The sampling frequency was 5120 Hz and the frequency resolution was 0.625 Hz. The data analysis utilized two different measurement-points combinations for each frequency; and each combination had 9–11 measurement points.

Fig. 5 shows the complex modulus estimation results obtained using the COE and the LS methods. The wave coefficients difference error from the COE method and the least-squares error from the LS method are plotted in Fig. 6.

Fig. 5 clearly shows the frequency dependence of the complex modulus of the PMMA. The real modulus increases sharply from 3.4 GPa at 30 Hz to 4.4 GPa at 100 Hz. After that it continues increasing, though more slowly, and it reaches approximately 4.9 GPa at 800 Hz. The loss factor increases with the increase of the frequency until it arrives at a maximum 0.065 at 80 Hz, and then it decreases gradually to approximately 0.043 at 800 Hz.

As shown in Fig. 5, the LS and the COE methods yield almost identical results for the complex modulus, except in the vicinity of 350 Hz, where both real modulus and loss factor curves show discontinuous behavior, and both COE error and the LS error are notably large.

It is interesting to compare the results of the current investigation with those published by Hillström et al., who originated the LS method employed here. Fig. 7 shows the current results alongside those presented in Ref. [10]. Notice that Hillström's results appear to have a large degree of error and that, other than that they are within the same order of magnitude, there is no clear trend in the data at these low frequencies. It is likely that the difference in the quality of the results arises from the differing measurement techniques used. The scanning laser vibrometer used for this study provides high-accuracy, non-contacting velocity measurements; whereas Hillström et al. used strain gauges in their testing. In addition, Hillström et al. performed their experiments on a non-uniform beam using the lateral impact excitation of a dropping steel ball, as opposed to the uniform beam configuration and steady sinusoidal excitation in this paper. Use of the vibrometer and steady-state excitation greatly improves the signal-to-noise ratio of the wave filed measurement and, consequently, increases the estimation accuracy.

7. Method validation and analysis

In the next sections, the PMMA results are compared with results from the literature and with results obtained experimentally using more complicated and restrictive conventional vibrating-beam techniques. Also presented is an investigation of the performance of the method in the low-frequency range (below 80 Hz) and in the vicinity of 350 Hz.

7.1. PMMA results comparisons

Koppelmann [14] performed a detailed test on a PMMA material near 25 °C. He used a cantilever beam setup and an impedance approach that exploited the relationship between stress and strain (or force and displacement). The results are plotted in Fig. 8 along with those obtained by using the COE and the LS methods.

As seen in Fig. 8, the real modulus estimation results from the COE and the LS methods compare well to those of Koppelmann. The differences between the current results and Koppelmann's become larger as frequency decreases below 70 Hz. Fig. 8 also shows that the COE and the LS method loss factor results are similar to Koppelmann's for frequencies higher than 80 Hz, where the loss factor decreases as frequency increases. Koppelmann's values for loss factor are consistently larger by roughly 0.01 within this range. Also

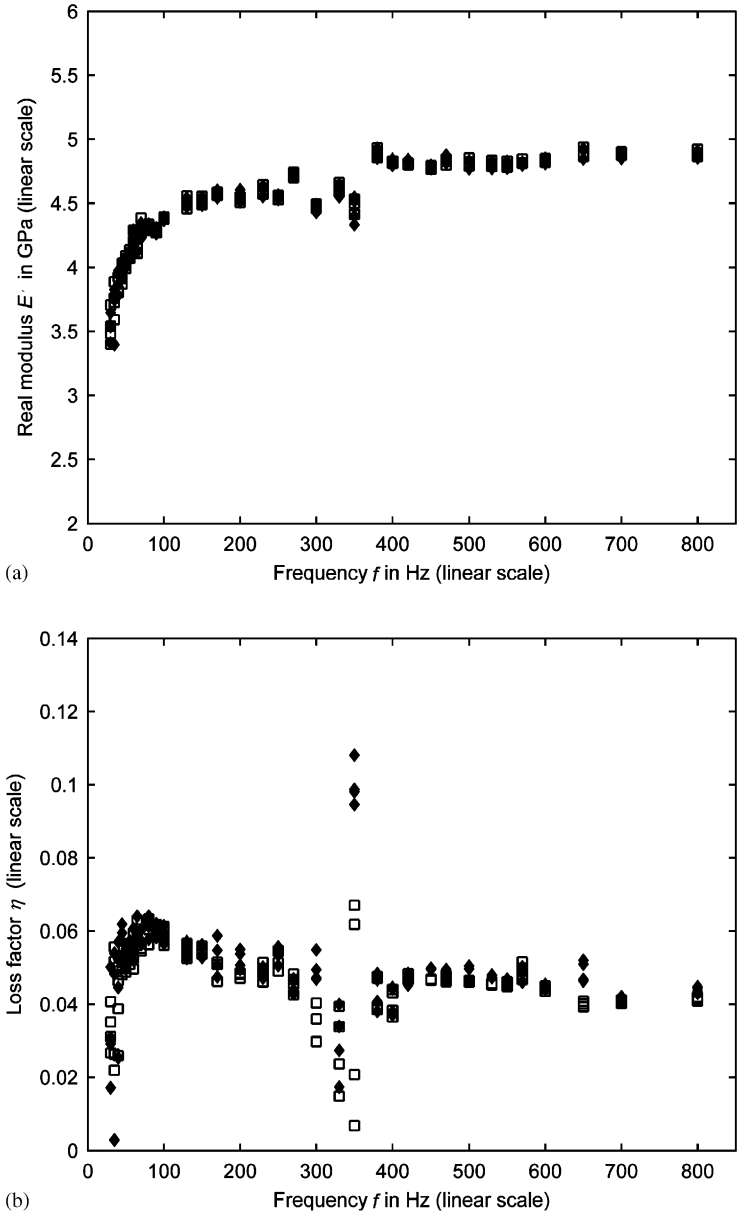

Fig. 5. Complex modulus E vs. frequency f for polymethyl methacrylate (PMMA). (a) Real modulus E'; (b) loss factor η. ◆, Wave coefficients (COE) method results; □, Least-Squares (LS) method results results.

notable is that, as in the case of the real modulus results, the differences in both value and trend become much larger as the frequency decreases below 80 Hz.

There are four possible explanations for the discrepancies between the results. First, and probably the most likely, is that, though Koppelmann's test material was also PMMA, its composite mixture properties can be quite different because of the manufacturing process. Secondly, Koppelmann performed the measurements at a temperature approximately 2.5 °C higher than the current experiments, which theoretically would produce a larger loss factor [15]. Third, it is always possible that the methods (COE and LS) are in error. Lastly, it could be the instrumentation or system error. In order to validate the results and find out the cause of the

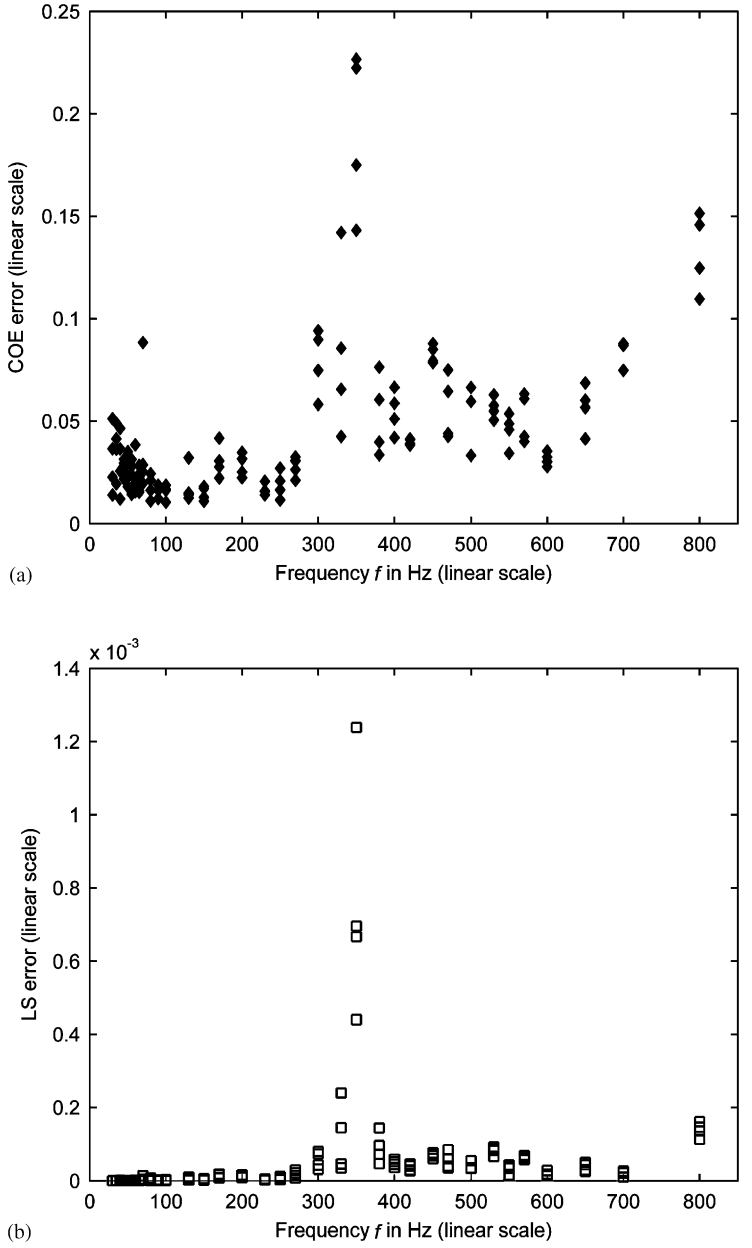

Fig. 6. Error e vs. frequency f for polymethyl methacrylate (PMMA). (a) ◆, Wave coefficients (COE) method error as defined in Section 2; (b) □, Least-Squares (LS) method error as defined in Section 3.

discrepancy, two conventional vibrating-beam techniques for estimating loss factor were applied to the beam, and the results are presented in the following sections.

To verify the loss factor results, the loss factor of the PMMA test beam was evaluated by the log decrement method. The log decrement method is a time-domain technique that is often utilized to measure damping ratios of vibratory systems. An impact hammer excited the free response of the test PMMA beam with clamped–free boundary conditions, whose decay envelope (or amplitude ratio) was then used to extract the damping ratio. The loss factor was calculated by utilizing the fact that loss factor is approximately twice the damping ratio at damped modal frequencies for small damping.

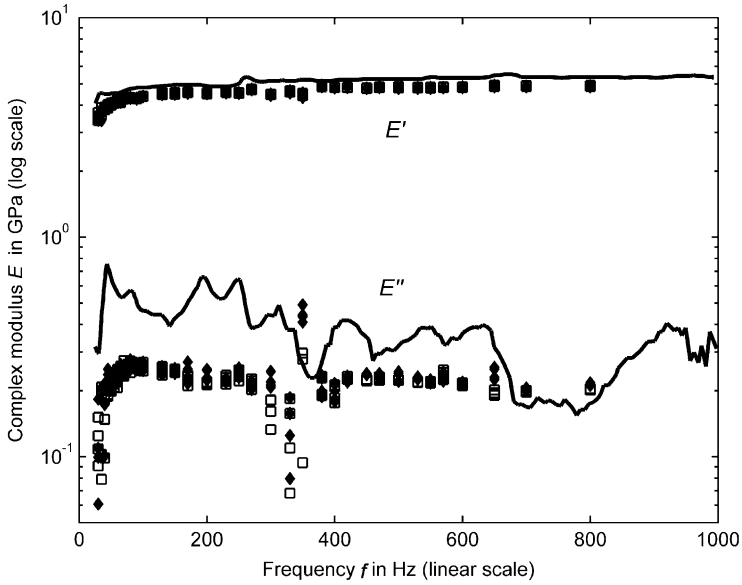

Fig. 7. Complex modulus $E = E' + iE''$ vs. frequency f for polymethyl methacrylate (PMMA). ◆, Wave coefficients (COE) method results (near 22.5 °C); □, Least-Squares (LS) method results (near 22.5 °C); ▬ Hillström et al.'s results (near 21.8 °C) [10] using the lateral impact excitation of a dropping steel ball and measurements from 8 strain gauges.

Theoretically the free response is a sum of sinusoidal waves at all modal frequencies. To estimate the loss factors at resonance frequencies other than the fundamental frequency, band-passing techniques were used to separate the waves and then log decrement method was applied to the isolated signals to evaluate the loss factor.

Because the log-decrement method can only be used to find damping at modal frequencies, the cantilever length of the test beam was varied by clamping it in various locations along the beam in order to change the frequencies of the natural modes. This makes possible the estimation of the loss factor at a large number of frequencies.

Fig. 9 shows the log decrement method results for the PMMA beam. The cantilever length was varied nine times from 0.34 to 0.16 m, by 0.02 m each time. The temperature was near 22.5 °C. The sampling frequency of the vibrometer was 5120 Hz.

The results were curve-fit using a second-order ARMA model, i.e., $\eta = (b_0 + b_1 f + b_2 f^2)/(1 + a_1 f + a_2 f^2)$ to yield a better presentation of the results for comparisons in the late part of this section.

As an additional verification of the loss factor results, the half-power bandwidth method, another of the conventional damping-ratio estimating techniques, was performed on the PMMA beam at a temperature near 23 °C. An impact hammer was used to excite the beam and then the free response was measured at 16 different locations along the beam. Forty measurements were taken at each beam location. The PSV 200 software calculated the transfer function between the impact force and the vibration velocity, and averaged all the transfer function spectra to obtain a mean transfer function spectrum, on which the half-bandwidth method was applied to estimate the loss factor.

Fig. 10 shows the transfer function spectrum of the beam. One may observe that the spectrum is not clean, and this makes damping estimation difficult. The 'uncleanness' is mostly due to the noisy signal from the hand-held hammer, especially at low frequencies. Since only a rough estimation of the loss factor is needed for comparison purposes, the half-band bandwidth method was applied to the average free response spectrum instead, which is shown in Fig. 11.

To improve the frequency resolution of the spectrum, and consequently to improve the accuracy of the loss factor estimates, the zero padding technique was used. First the averaged spectrum at each measurement

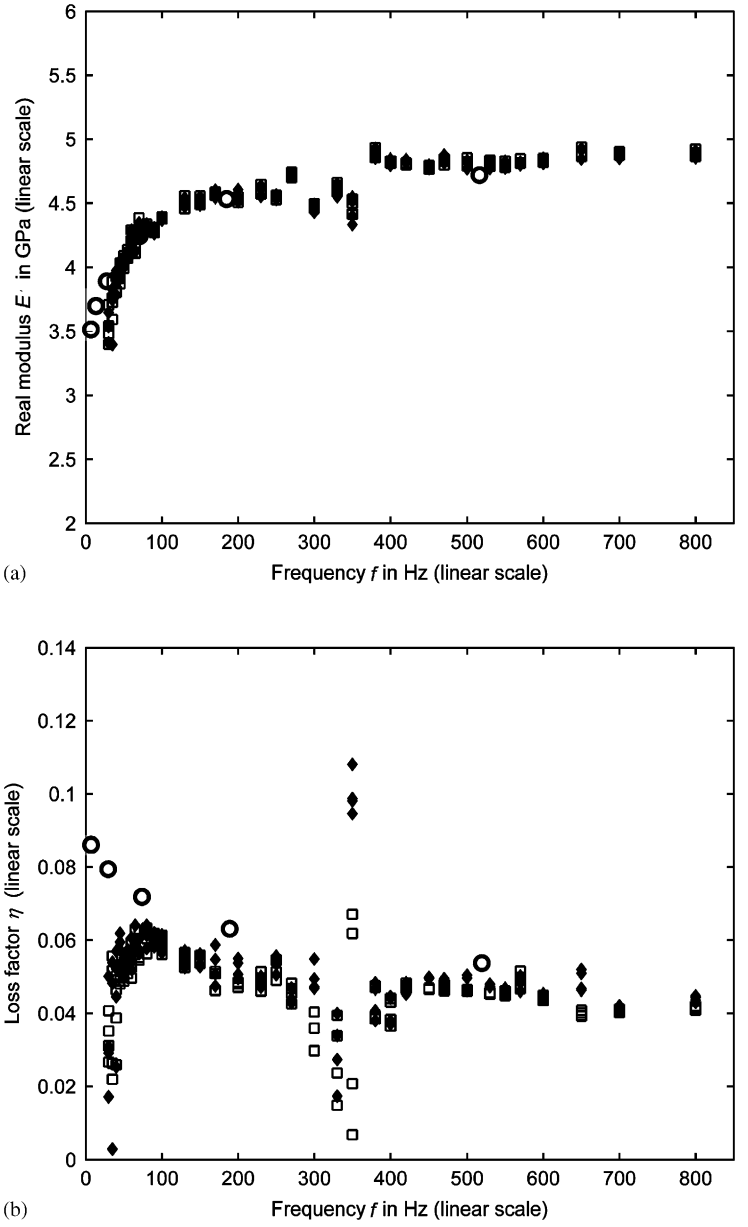

Fig. 8. Complex modulus E vs. frequency f for polymethyl methacrylate (PMMA). (a) Real modulus E'; (b) loss factor η. ◆, Wave coefficients (COE) method results (near 22.5 °C); □, Least-Squares (LS) method results (near 22.5 °C); ○, Koppelmann's results (near 25 °C) [13].

location was transformed to obtain a time domain signal of 6400 points (or of a time interval of 1.6 s). Then the time domain signal was zero padded to 130,672 points (or of a time interval 32.668 s). Then an FFT was applied to the zero-padded time trace to yield a frequency spectrum for this measurement location. Finally, all the spectra at different locations were averaged.

Table 2 shows that in the frequency range of interest the loss factor of the PMMA beam varies from 0.05 to 0.08, which is slightly larger than the results of Section 6. At low frequencies the resonance peak is much sharper (or the half-power-bandwidth is much narrower), and this makes it very difficult for the data

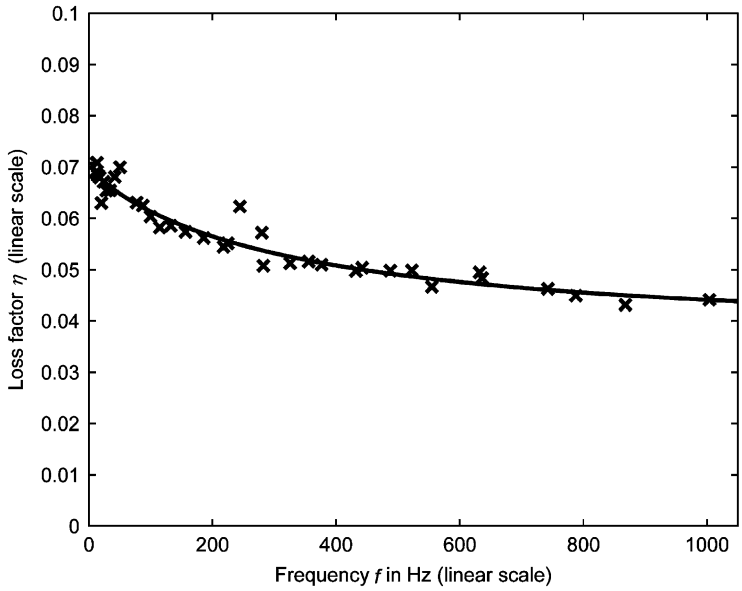

Fig. 9. Loss factor η vs. frequency f for polymethyl methacrylate (PMMA) near 22.5 °C. ×, log decrement results; ▬, curve-fitted log decrement results.

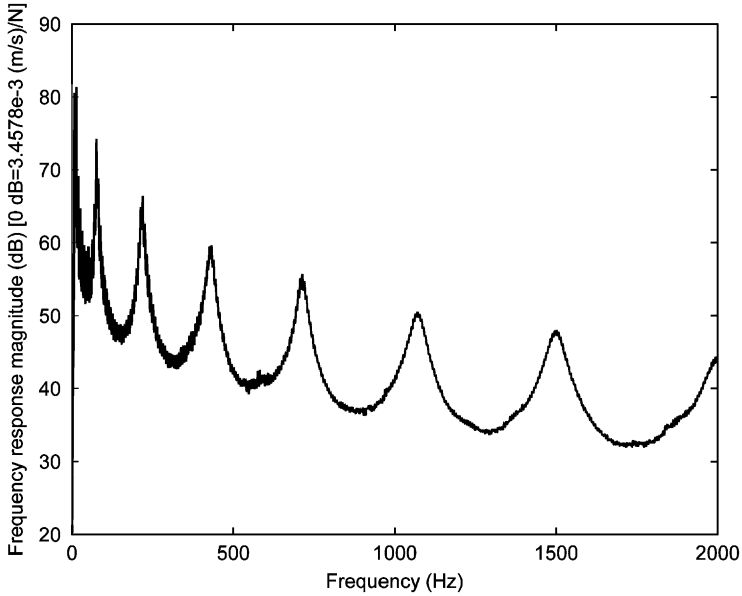

Fig. 10. Transfer function spectrum of the modal testing PMMA beam system.

acquisition system to capture the exact resonance peak; therefore, the half-power bandwidth is exaggerated at very low frequencies and the loss factors are amplified. Moreover, the idea of the half-power bandwidth method is to treat resonance frequencies individually as if from single-degree-of-freedom (SDOF) systems. As the resonance frequency increases, the superposing effect of the low-frequency SDOF systems becomes more significant and this will also cause the estimate to be larger than the actual loss factor. Near the 5th modal

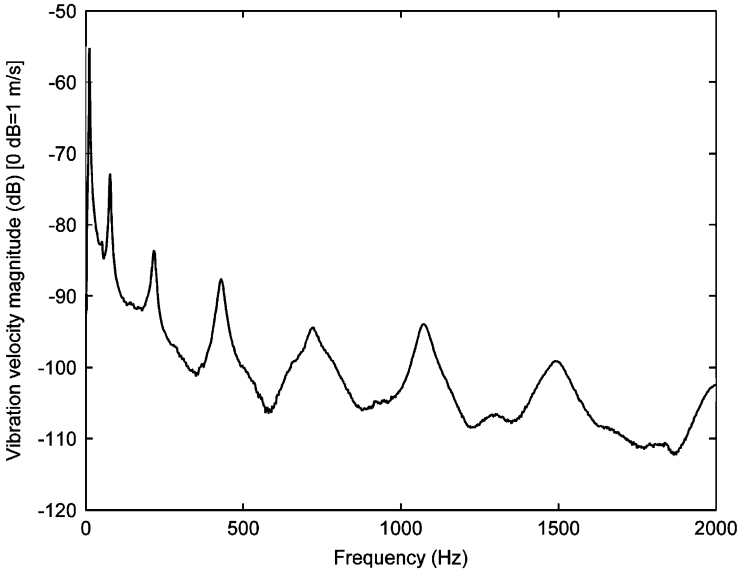

Fig. 11. Free response spectrum of the modal testing PMMA beam system.

Table 2
Experimental modal frequencies and loss factor estimates from modal testing

Mode number	Experimental resonance frequency (Hz)	Estimated loss factor
1	11.7	0.140
2	77.1	0.074
3	216.7	0.065
4	429.6	0.056
5	720.8	—
6	1071.7	0.049

frequency, 720.8 Hz, the frequency spectrum measurement is not of high enough quality to accurately estimate the loss factor.

The loss factor results obtained by using the COE, LS, the log decrement and half-power bandwidth methods, along with Koppelmann's results, are compared in Fig. 12. Fig. 12 shows that at frequencies higher than 80 Hz, the COE and the LS results are close to those estimated using the log decrement method. Koppelmann's loss factors roughly follow the log-decrement loss factor curve, with Koppelmann's being approximately higher by 0.01.

As frequencies decreases below 80 Hz, the difference, between the results obtained by the COE and LS methods and those obtained by the log decrement and half-power bandwidth methods and Koppelmann, becomes larger. The real modulus from the COE and LS methods drops much faster than Koppelmann's. The loss factor estimated by the COE and LS method goes down quickly as frequency decreases, as opposed to the increasing trend shown in the results obtained by other methods.

Physically, the low-frequency failure of the COE and LS methods is due to the fact that as the frequency decreases the bending motion of the beam becomes smaller, in other words, the magnitude and phase curves of the wave field are more flat. Since the COE and LS methods essentially utilize the magnitude and phase differences among the vibration velocity measurements at different locations on the beam to

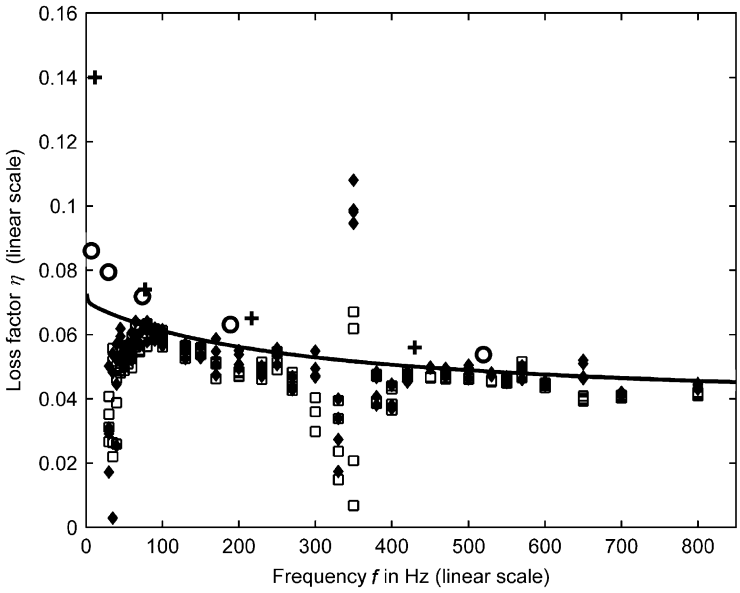

Fig. 12. Loss factor η vs. frequency f for polymethyl methacrylate (PMMA). ◆, Wave coefficients (COE) method results (near 22.5 °C); □, Least-Squares (LS) method results (near 22.5 °C); ▬, curve-fitted log decrement method results (near 22.5 °C); +, half-power bandwidth method results (near 22.5 °C); ○, Koppelmann's results (near 25 °C).

estimate the wavenumber, at low frequencies the differences are very small and a small measurement error can lead to large errors in the wavenumber estimation. This low-frequency degradation will be further studied in Section 7.2.1.

7.2. PMMA results investigation

7.2.1. Numerical error analysis

The above result comparisons show that the COE method was able to accurately measure the complex modulus of PMMA except at frequencies below 80 Hz and near 350 Hz. The LS method performed similarly overall, including displaying similar inaccuracies in the same frequency ranges. To investigate the cause of the estimation problems in these areas, a numerical error analysis was carried out to test the performance of the methods.

As in the error analysis for the aluminum experiments in Section 5, first the LS method was used to estimate the complex wavenumber from an experimental wave field measurement at a specific frequency. The corresponding 'optimized' wave coefficients were computed for this complex wavenumber. Then the real part of the wavenumber was fixed but its imaginary part was adjusted to a value that would make the corresponding complex modulus' loss factor to be 0.06. This complex wavenumber and the 'optimized' wave coefficients were used to numerically construct a new wave field, which was very close to the original real wave field measurement but had a known wavenumber. Then random Gaussian noise, which had the same specifications as in Table 1, was added to the new wave field measurement. Finally, the LS and the COE methods were applied to these simulated data.

The process was repeated 500 times for each experimental wave field measurement and the statistics of the results are presented in Fig. 13, where $e_{E'}$ is the normalized real modulus estimation error as defined in Eq. (9), and e_η is the loss factor estimation error defined as

$$e_\eta = \sqrt{\frac{1}{R}\sum_{r=1}^{R}(\eta_{\mathrm{Est}} - 0.06)^2}, \tag{11}$$

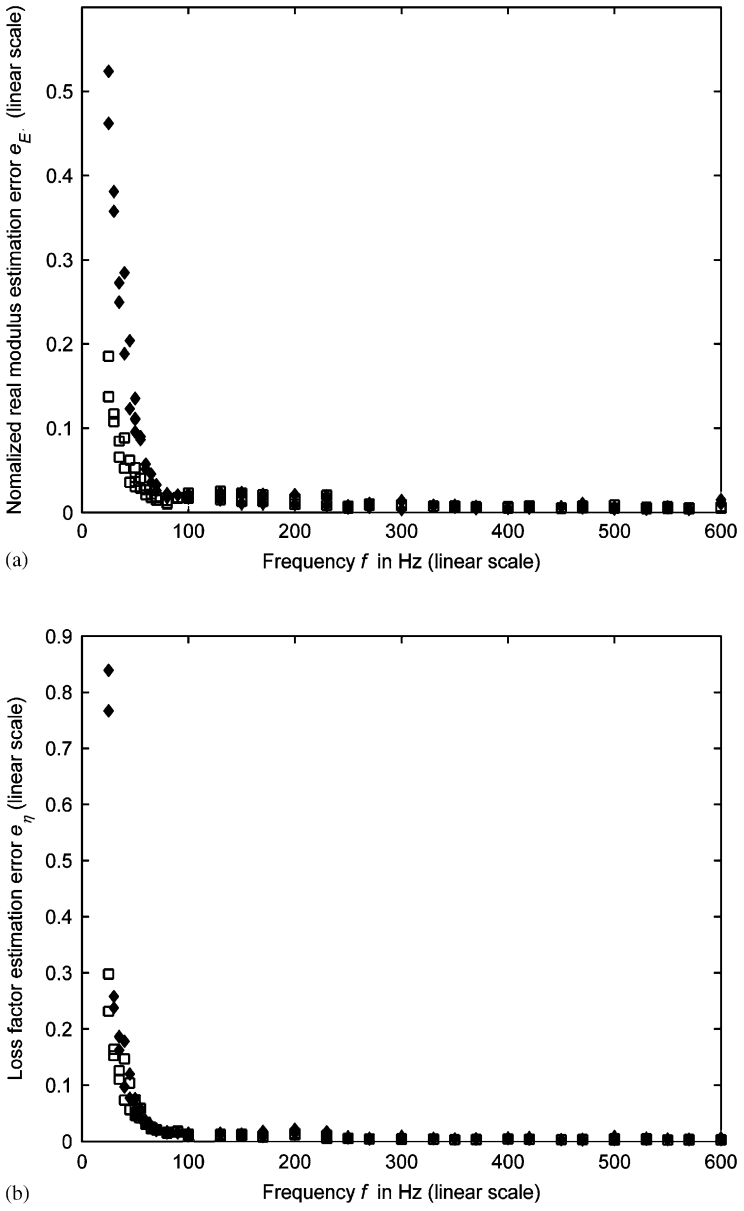

Fig. 13. Complex modulus estimation error vs. frequency f for estimating simulations of the PMMA beam with cantilever length 0.34 m. (a) Normalized real modulus estimation error $e_{E'}$; (b) loss factor estimation error e_η; ◆, Wave coefficients (COE) method; □, Least-Squares (LS) method.

where η_{Est} is the loss factor estimated from the noise-added measurement, and the total number of Monte-Carlo simulations, R, is 500.

The error analysis results are also plotted in Fig. 14 on a different scale to yield a more detailed view of the errors at frequencies higher than 100 Hz.

Figs. 13 and 14 show generally that the estimation error decreases as the frequency increases. The estimation errors of both methods are relatively small at frequencies higher than 200 Hz, below 1% for real modulus estimation and less than 0.005 for loss factor estimation. However, the error increases dramatically as the frequency decreases below 80 Hz. In the low-frequency area, the real modulus

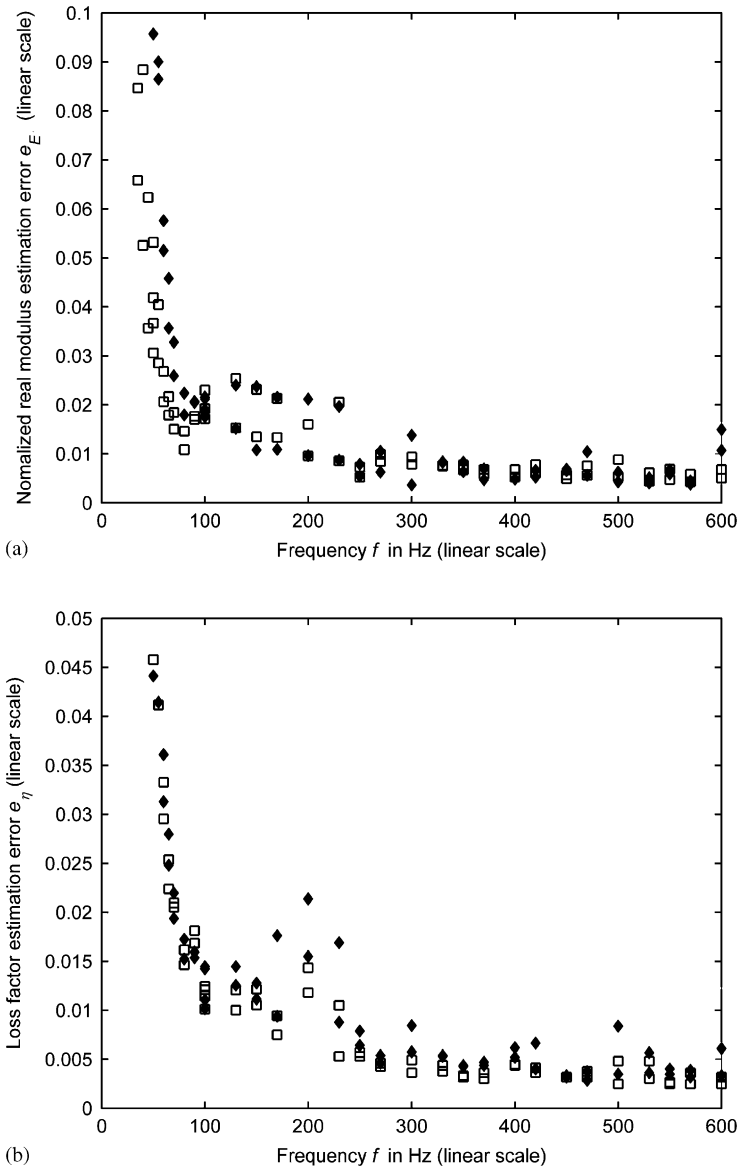

Fig. 14. (Zoom-in view of Fig. 13.) Complex modulus estimation error vs. frequency f for estimating simulations of the PMMA beam with cantilever length 0.34 m. (a) Normalized real modulus estimation error $e_{E'}$; (b) loss factor estimation error e_η; ◆, wave coefficients (COE) method; □, Least-Squares (LS) method.

estimation error of the LS method is smaller than that of the COE method, while for loss factor estimation they have comparable performances. It is noticeable that the errors are smaller than those for the aluminum simulation case as shown in Fig. 4. One reason is that more measurement points were used for the PMMA estimation.

Plotted in Fig. 15 are the averages of the normalized real moduli and loss factors in the error analysis. $\mu_{E'}^{\mathrm{Nor}}$ is the normalized real modulus average defined as $(\sum_{r=1}^{R} E'_{\mathrm{Est}})/(RE'_{\mathrm{Sim}})$ and μ_η is the loss factor average defined as $\sum_{r=1}^{R} \eta_{\mathrm{Est}}/R$. The figure shows that as frequency decreases the average of the real modulus estimates becomes increasingly lower than the simulated real modulus. This suggests that, because of the effect of measurement noise, at low frequencies the methods tend to underestimate the real modulus, which is in

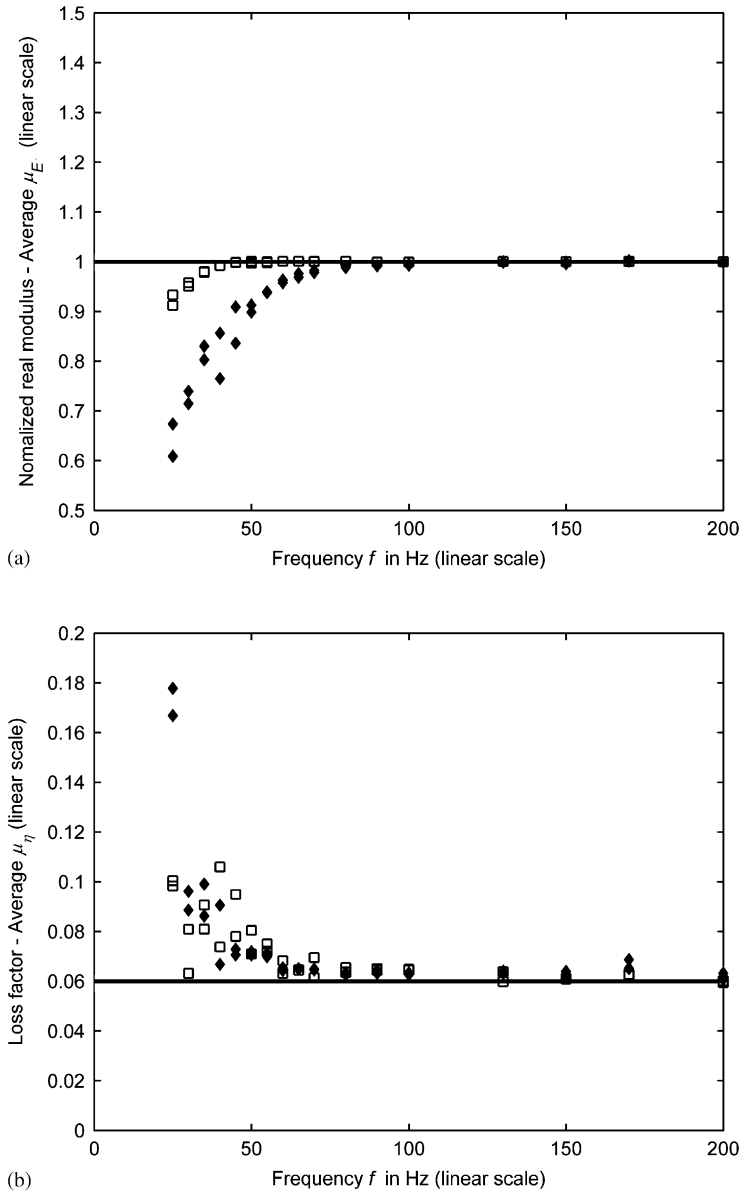

Fig. 15. Averages of the normalized real modulus and loss factor estimates for estimating simulations of the PMMA beam with cantilever length 0.34 m. (a) $\mu_{E'}$, normalized real modulus average; (b) μ_{η}, loss factor average. ◆, Wave Coefficients (COE) method; □, Least-Squares (LS) method.

agreement with the experimental results in Section 6. However, the figure also suggests that the methods could more likely overestimate the loss factor at low frequencies and this is contradictory with the experimental loss factor results.

A tentative physical explanation for the underestimating problem of the loss factor at low frequencies is as follows. The loss factor is strongly related to the phase differences among the measurement points. At low frequencies, the phase differences become much smaller, and errors in the phase measurements may be comparable or even larger than the differences. At some limit, the phase difference corrupted by the noise appears numerically the same as the noise itself or as the zero phase-difference plus the noise. Note that zero

phase-difference corresponds to a loss factor of zero. Therefore, the methods could mistake the noise-corrupted wave field for one with a loss factor lower than it actually has.

The above analysis shows that both methods show difficulties in estimating accurately at low frequencies. Therefore, the discrepancy between loss factor results of the COE and the LS methods and those of the log decrement method at low frequencies was caused due to the estimation limitations of the COE and the LS methods.

One may suggest that using an error function including the coefficients c and d might improve the estimation accuracy of the COE method and its performance at low frequencies. However, as shown in Appendix A, including c and d in the error function actually degrades the estimation performance. The main reason is that c and d are wave coefficients associated with low signal-to-noise ratio measurements. Appendix A shows that the magnitudes of a, b, c and de^{kL} are comparable to each other, where L is the beam length. If the system is of low damping, the magnitudes of the dominant wave terms ae^{-ikx} and be^{ikx} stays fairly constant along the test beam. However, the magnitude of the near-field term ce^{-kx} decreases exponentially as x increases from 0 to L, while the magnitude of the other near-field term de^{kx} drops exponentially as x decreases from L to 0. If the real part of the wave number is large (i.e., high frequency), or the beam is long, or both, the wave field in the middle (or most area) of the beam are dominated by the ae^{-ikx} and be^{ikx} wave components and it has very little contribution from the ce^{-kx} and de^{kx} terms.

One way to improve the performance of the estimation methods at low frequencies is to increase the distances between the measurement points. Fig. 16 shows the estimation results from simulations of a clamped–free PMMA beam with a cantilever length of 0.68 m.

To obtain noise-free wave fields for the simulations, first at a specific or known frequency (or wavenumber) the wave coefficients were determined by using boundary conditions (see Appendix B). Then the wave-number and the determined wave coefficients were used to construct the noise-free wave fields. The total number of measurement points was the same as that for error analysis of the PMMA beam with cantilever length 0.34 m, but the points were chosen in a way that made the distances twice the previous ones. For example, at 200 Hz one set of measurement points for the 0.34 m PMMA beam was chosen as [0.02, 0.05, 0.08, 0.11, 0.14, 0.20, 0.23, 0.26, 0.32] m; the corresponding measurement point set for the 0.68 m PMMA beam was located at [0.04, 0.10, 0.16, 0.22, 0.28, 0.40, 0.46, 0.52, 0.64] m. After that, the magnitudes of the vibration velocities at these measurement points were scaled to make the total measured vibration energy close to that of the measurement points for the 0.34 m PMMA beam, i.e., $\left[\sum_{i=1}^{N}|\hat{v}_i|^2\right]_{0.64\,\mathrm{m}} \cong \left[\sum_{i=1}^{N}|\hat{v}_i|^2\right]_{0.32\,\mathrm{m}}$, where N is the total number of measurement points. Random Gaussian noise was then added to the noise-free wave field. The added noise had the same specifications as in Table 1. Finally, the LS and the COE methods were applied for estimation.

Comparison of Figs. 13 and 16 shows that the estimation accuracy has improved significantly by increasing the distances between the measurement points. For the 0.34 m PMMA beam case, as the frequency decreases from 100 to 25 Hz, the normalized real modulus estimation error $e_{E'}$ increases from about 0.02 to 0.20 and the loss factor estimation error e_η increases from around 0.015 to 0.30. For the 0.64 m PMMA beam case, $e_{E'}$ is less than 0.02 and $e_\eta$is less than 0.015 overall in the same frequency range. Moreover, $e_{E'}$ is less than 0.01 and e_η is less than 0.005 in the frequency range 60–100 Hz.

The error analysis shows that both of the LS and the COE estimation methods have limitations in estimating the complex modulus at low frequencies. However, the numerical error analysis does not show any estimating problems in the near-350 Hz frequency area, which is further investigated below.

7.2.2. Results of PMMA beams with different dimensions

The numerical error analysis shows that the COE and the LS methods themselves were not the origin of the estimating inaccuracy at frequencies around 350 Hz. Moreover, as shown from the modal testing results in Table 2, no resonance frequency of the transverse vibrations lies in the near-350 Hz region. One may suggest that the problem could be caused by the model error, because the LS and the COE methods both use a beam model only considering bending waves, however, other types of vibrations

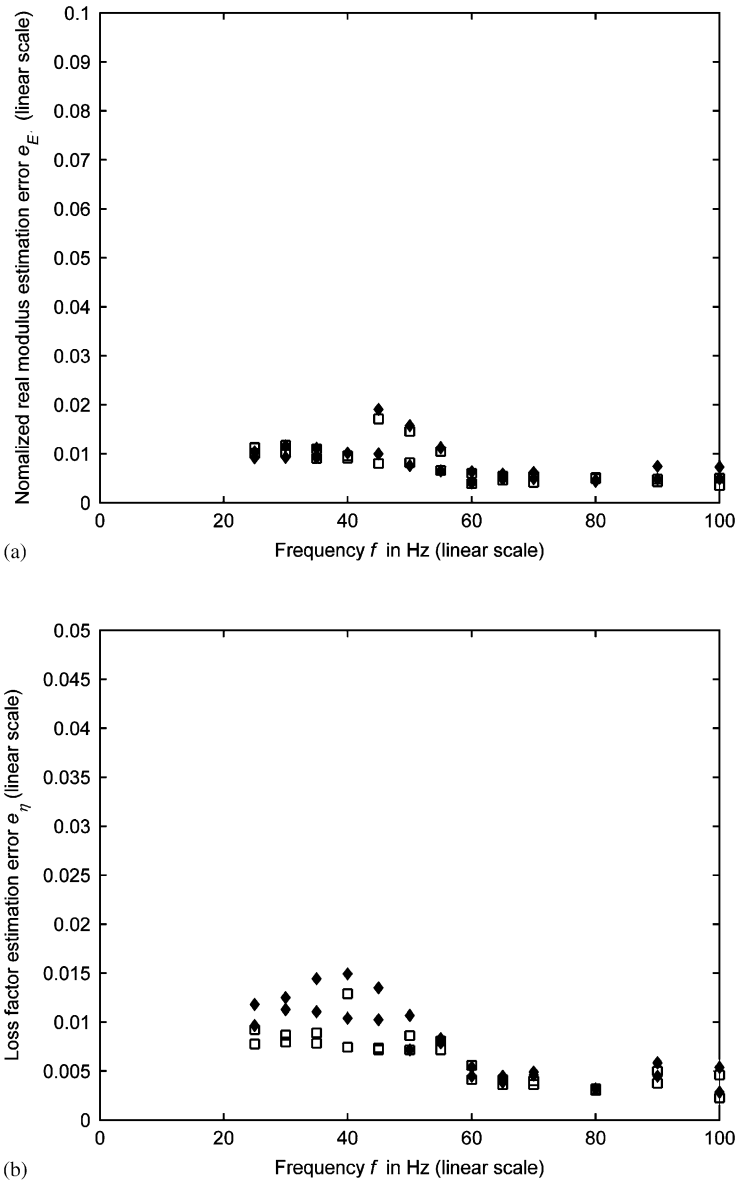

Fig. 16. Complex modulus estimation error vs. frequency f for estimating simulations of a simulated clamped-free PMMA beam with cantilever length 0.68 m. (a) Normalized real modulus estimation error $e_{E'}$; (b) loss factor estimation error e_η; ◆, Wave Coefficients (COE) method; □, Least Squares (LS) method.

could be excited in experiments, such as torsional modes and plate modes. To examine the effects of those modes, experiments were performed on two other PMMA beams with different dimensions but made from same material sample and the results are shown in Figs. 17 and 18. Beam *a* was the beam used to obtain the results in Section 6. Beams *b* and *c* are beams with the same thickness but different width or length, respectively. Table 3 shows the dimensions of the beams. Also presented in Table 3 are the theoretical natural frequencies of the first two torsional modes of the PMMA beams calculated using Blevins' formula [16].

Fig. 17 shows that the results of the three beams are very close except in the neighborhood of 350 Hz, where all of them show irregularity and both of the COE and the LS errors are considerably larger than those at

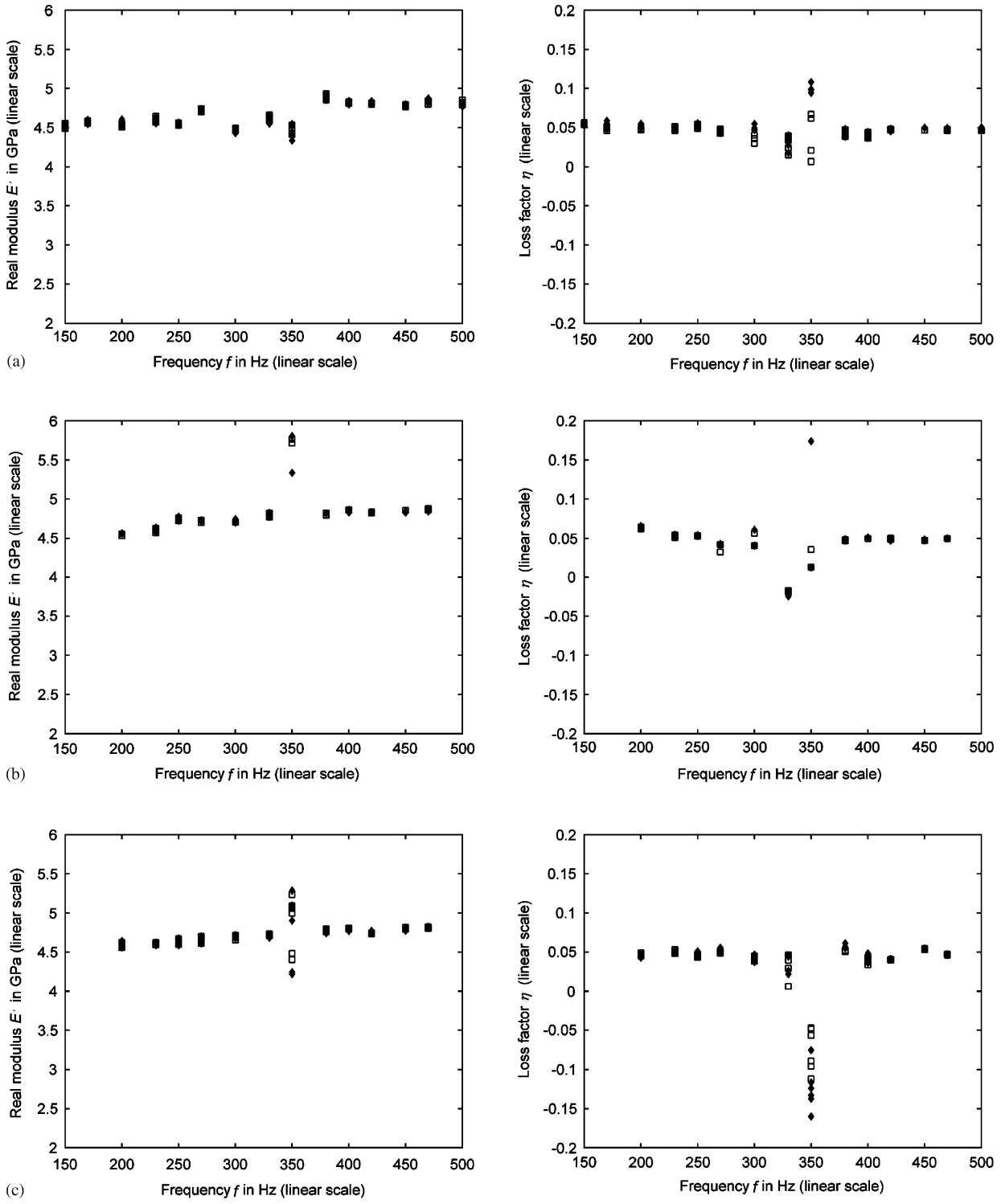

Fig. 17. Real modulus E' and loss factor η vs. frequency f for polymethyl methacrylate (PMMA). ◆, Wave coefficients (COE) method results; □, Least-Squares (LS) method results. (a) Beam dimensions: length, 340 mm; width, 20 mm; thickness, 4.42 mm. (b) Beam dimensions: length, 340 mm; width, 15 mm; thickness, 4.42 mm. (c) Beam dimensions: length, 300 mm; width, 20 mm; thickness, 4.42 mm.

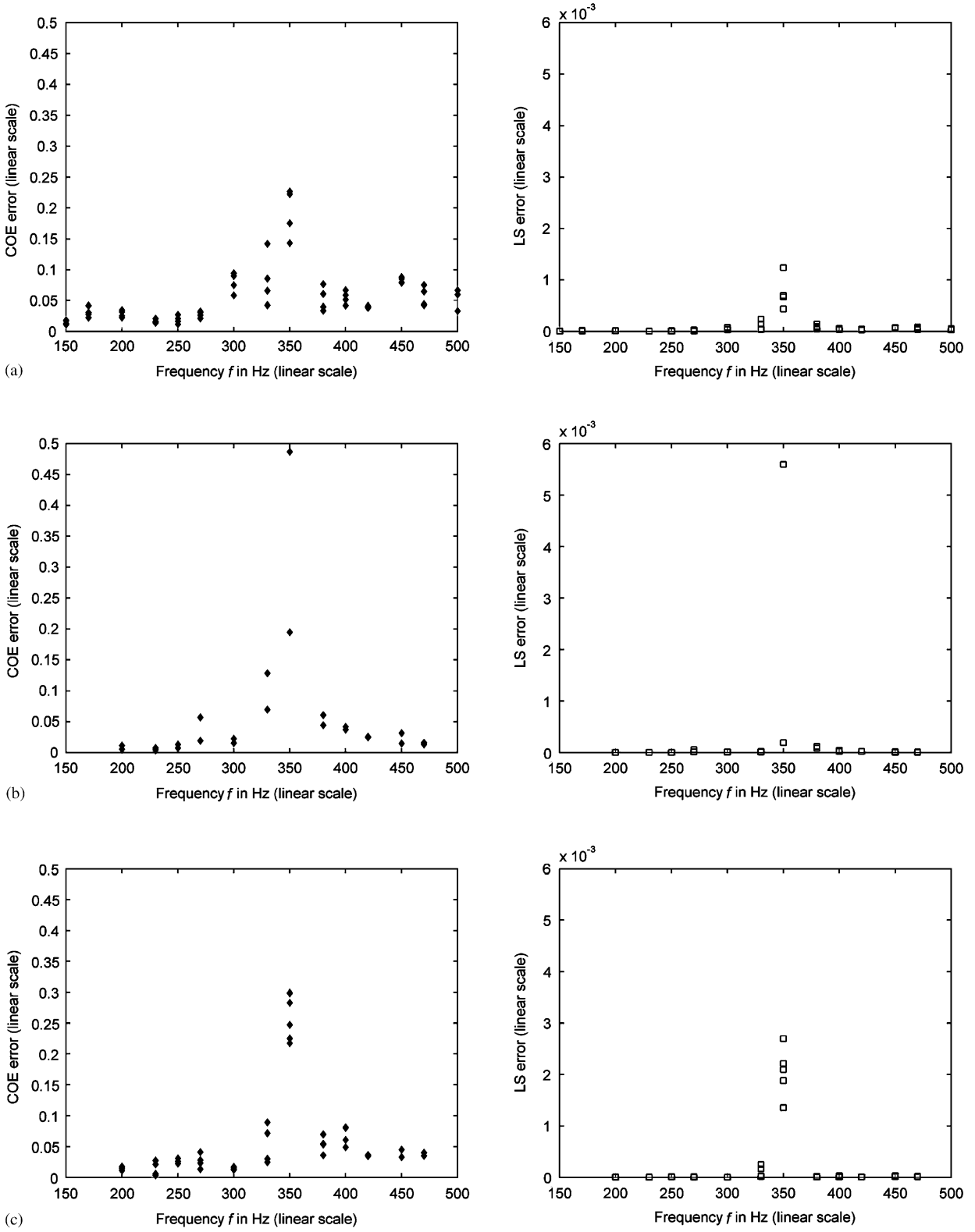

Fig. 18. Error e vs. frequency f for polymethyl methacrylate (PMMA). ◆, Wave coefficients (COE) method error as defined in Section 3; □, Least-Squares (LS) method error as defined in Section 4. (a) Beam dimensions: length, 340 mm; width, 20 mm; thickness, 4.42 mm. (b) Beam dimensions: length, 340 mm; width, 15 mm; thickness, 4.42 mm. (c) Beam dimensions: length, 300 mm; width, 20 mm; thickness, 4.42 mm.

Table 3
Torsional modal frequencies using Blevins' formula [16]

PMMA beam	Length (mm)	Width (mm)	Thickness (mm)	1st modal frequency (Hz)	2nd modal frequency (Hz)
a	340	20	4.42	347.6	1108.5
b	340	15	4.42	447.3	1434.2
c	300	20	4.42	394.0	1182.0

other frequencies. Since the first torsional frequency for beam *a* occurs at approximately 348 Hz, it was originally thought that the errors near 350 Hz were a result of exciting the beam near a resonance. However, the problem frequency remained at 350 Hz regardless of which beam was being tested. Resonances were eliminated as a cause of the prediction error.

7.2.3. Resonance phenomenon of the vibrometer

Velocity measurements were taken on the top surface of the beam clamp at a location very close to the accelerometer while the shaker was powered off. The frequency spectrum of the measured signals by the accelerometer and the vibrometer, respectively, were obtained. Overall they are spectrums typical of random noise. However, the vibrometer signal spectrum shows significant peaks at frequencies close to 350, 825 and 1215 Hz, which do not appear in the spectrum of the accelerometer signal.

An acoustic experiment was performed to check the resonance of the vibrometer. Measurements were taken by the vibrometer on an aluminum beam lying vertically against the lab wall. To rule out the structural effects of the supporting frame of the vibrometer on the measurements, the scanning head of the vibrometer was removed from its supporting frame and sits horizontally on the lab floor with its corners supported by rubber isolators to cut-off or reduce the excitation from the ground. A mistuned AM radio was used as the source to generate pseudo-white noise. Two speakers were put nearby and facing the vibrometer head. Fig. 19 shows the power spectral density of the measurements with and without the pseudo-white noise excitation.

As shown in Fig. 19, though magnitudes of most of the frequency components increased less than 25 dB, the one around 345 Hz is boosted by about 55 dB, from -130 to -75 dB approximately. The peak near the 832 Hz increases by about 35 dB, from -125 to -90 db approximately.

All the above evidence leads to the conclusion that those resonance peaks in the spectrum are intrinsic characteristics of the vibrometer system.

7.2.4. Error investigation conclusions

The numerical error analysis shows that both the COE and the LS estimation methods have difficulty in estimating accurately at very low frequencies.

All experiments for both aluminum and PMMA samples showed irregularities at frequencies near 350 Hz, and further examination of the experimental results show errors in the modulus at around 800 Hz as well. Vibrometer measurements were then taken on the top surface of the motionless clamp at a location close to the accelerometer, while the shaker was powered off, and the spectrum of the measured signal shows resonance peaks at frequencies near 350, 825 and 1215 Hz.However, those peaks are not shown in the spectrum of the signal measured by the accelerometer. Another experiment was carried out to verify the resonance using acoustic excitation. The magnitudes of the peaks around 350 and 830 Hz increased much more significantly than those at other frequencies under pseudo-white noise acoustic excitation. Moreover, a careful examination of Fig. 6 shows that the COE and the LS errors become large again at 800 Hz while they are relatively small in the frequency interval 400–700 Hz.

Based on the above facts, it can be concluded that the vibrometer system has some noise-resonance-like phenomenon at frequencies close to 350, 825 and 1215 Hz. Near these frequencies a small change of the vibration velocity will induce a relatively larger change in the measurement as compared to

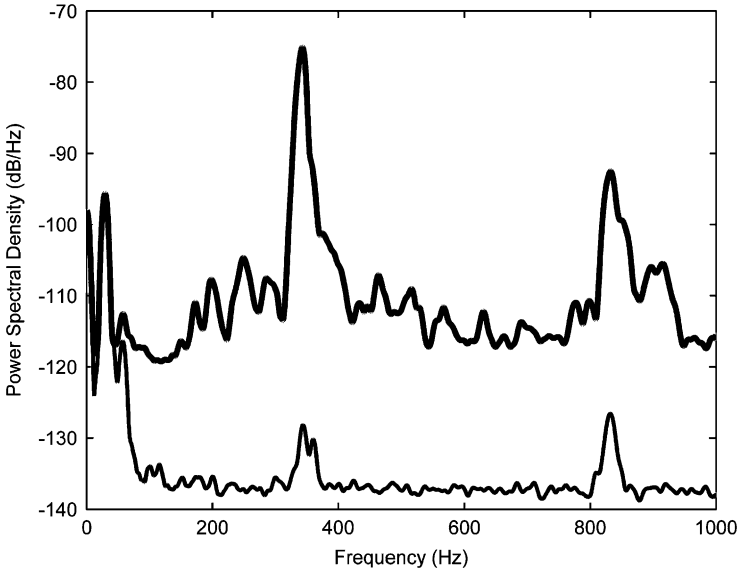

Fig. 19. Power spectral density of the signal measured by the vibrometer on an aluminum beam lying against a wall, with shaker power off. ▬, without pseudo-white noise acoustic excitation to the vibrometer scanning head; ●●●●, with pseudo-white noise acoustic excitation.

at other frequencies. In other words, the measurement error is amplified in those resonance areas. And this is the reason the COE and the LS methods had poor performances at the frequencies near 350 Hz.[1]

8. Conclusions

The COE method was developed to estimate the complex modulus of viscoelastic materials from measured data. It can be used to evaluate complex modulus at any frequency, and its application is independent of boundary conditions. The method does require that the beam model assumptions are satisfied. Another advantage of the COE method is that its experimental setup is simple to realize in practice.

The method was applied to a nearly undamped material, aluminum, and to a low-damping material, PMMA. The results are close to those obtained by using Hillström et al.'s LS method [8], and in good agreement with those in the literature. The results were also verified by using the half-power bandwidth method and the logarithmic decrement method.

Both the COE method and the LS method have difficulty in estimating accurately at very low frequencies. For the experimental setup used for this study, the results lose accuracy when the excitation frequency drops below the second modal frequency. However, the performance can be improved by using more measurement points, or by increasing the distance between the measurement points, or both. Estimation errors become smaller as frequency increases, or as the wavenumber increases. Therefore, reducing the thickness of the test beam helps to improve the estimation accuracy.

[1]Polytec, the manufacturer of the vibrometer, was contacted for technical support regarding the issue. After reviewing the data and investigation analysis, its Chief Technical Officer concluded that the peaks in the spectrum were most likely due to mirror resonances of the scanning vibrometers. This speculation was further confirmed by measurements performed on their own non-scanning and scanning vibrometers.

Table A1
Magnitudes of the wave coefficients in the PMMA experiments

Frequency (Hz)	$\|a\|$ (m/s)	$\|b\|$ (m/s)	$\|c\|$ (m/s)	$\|de^{kL}\|$ (m/s)
50	0.0184	0.0166	0.0345	0.0169
200	0.0226	0.0180	0.0343	0.0203
600	0.0181	0.0122	0.0294	0.0187

Because of an inherent resonance within the vibrometer system, the measurement error is relatively large at frequencies close to 350 Hz, and this caused the COE method and the LS method to have poor performances at that frequencies.

The using of a non-contacting scanning laser Doppler vibrometer and sinusoidal excitation provided by a shaker, as opposed to the strain gauge and impact excitation [10], greatly improves the quality of the results over those presented by Hillström et al.

As a final note regarding the experiments, though the estimation theory is based on measurements of the vibration velocities, experiments show that more accurate results were obtained by instead using the transfer functions between measurement points (response) and accelerometer (excitation) because the transfer functions provide a more accurate relationship among the measurement points if the excitation is not stable (or truly steady state). The aluminum and PMMA estimation results shown in this paper were obtained by measuring transfer functions.

Appendix A. Wave coefficients error function definition including the coefficients *c* and *d*

The new wave coefficients error function that includes the near-field coefficients c and d is defined as

$$e_{abcd}(k) = \frac{\sqrt{var(a_1, a_2, ..., a_Q)}}{|\text{mean}(a_1, a_2, ..., a_Q)|} + \frac{\sqrt{\text{var}(b_1, b_2, ..., b_Q)}}{|\text{mean}(b_1, b_2, ..., b_Q)|} + \frac{\sqrt{var(c_1, c_2, ..., c_Q)}}{|\text{mean}(c_1, c_2, ..., c_Q)|} + \frac{\sqrt{\text{var}(d_1, d_2, ..., d_Q)}}{|\text{mean}(d_1, d_2, ..., d_Q)|}. \tag{A1}$$

The identified magnitudes of a, b, c and de^{kL} from the experiments at some frequencies are given in Table A.1.

Same numerical error analysis as in Section 7.2.1 was carried out to compare the performance of the wave coefficients method with different error definitions. Figs. A1 and A2 show the estimation results obtained by the methods. The realization number r is the simulation index for the Monte-Carlo simulations. The simulated noise-free wave-field wavenumber $k = 9.2390 - \text{i}0.1386$ is corresponding to the actual PMMA experiment at 30 Hz, while $k = 27.4500 - \text{i}0.4195$ is corresponding to the 300 Hz PMMA experiment. For convenience, COE_{ab} is used to denoted the wave coefficients method whose error function (defined in Eq. (8)) includes only a and b and COE_{abcd} represents the method whose error function (defined in Eq. (A1)) includes all the wave coefficients.

Appendix B. Determing wave coefficients using boundary conditions

The boundary conditions are given by

$$\left.\frac{\partial \hat{y}}{\partial x}\right|_{x=0} = 0, \quad \left.-EI\frac{\partial^3 \hat{y}}{\partial x^3}\right|_{x=0} = \hat{F}_0, \quad \left.EI\frac{\partial^2 \hat{y}}{\partial x^2}\right|_{x=L} = 0, \quad \left.-EI\frac{\partial^3 \hat{y}}{\partial x^3}\right|_{x=L} = 0. \tag{B1}$$

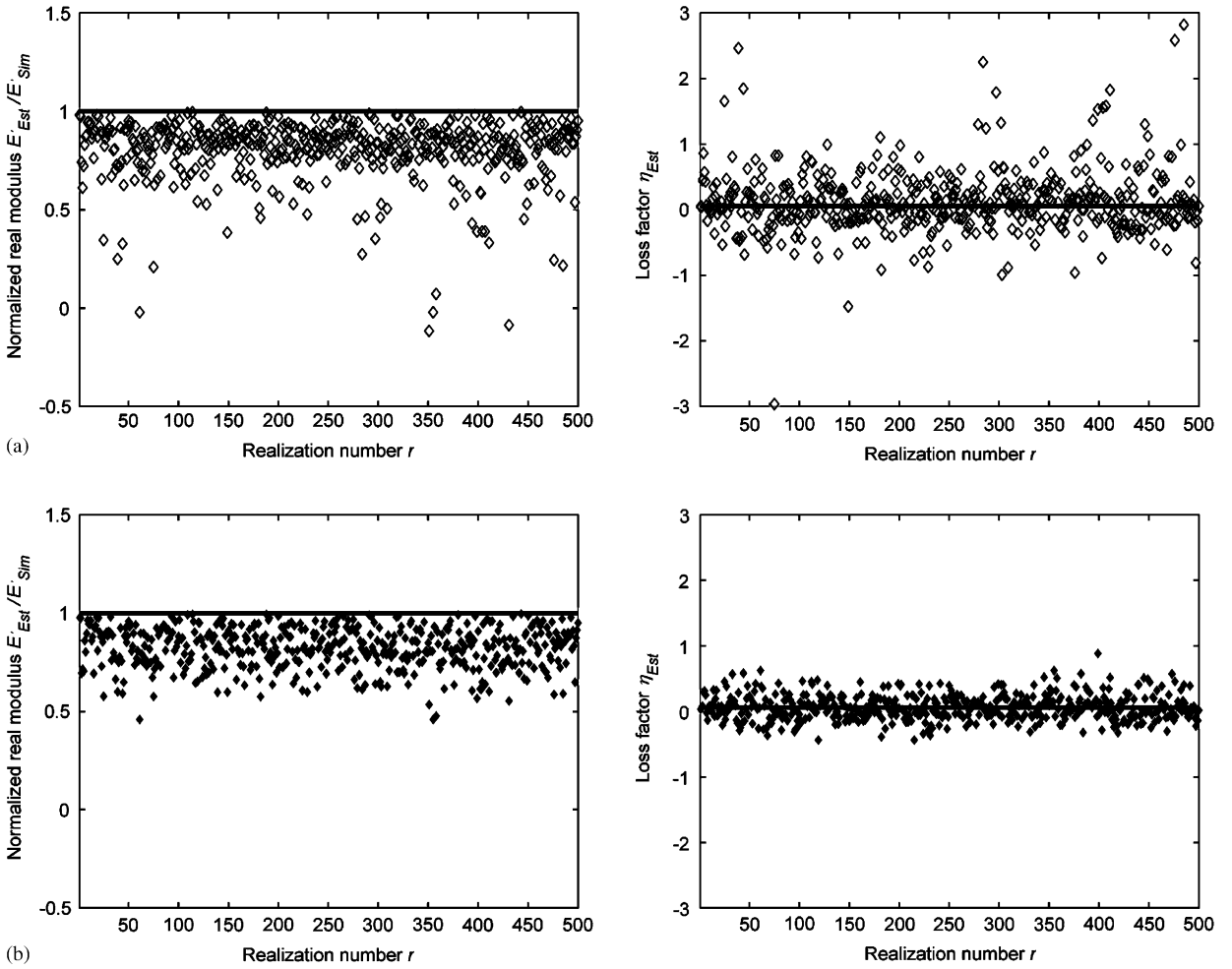

Fig. A1. Normalized real modulus $E'_{\mathrm{Est}}/E'_{\mathrm{Sim}}$and loss factor η estimates vs. realization number r for error analysis with noise-free wave-field wavenumber $k = 9.2390 - \mathrm{i}0.1386$. (a) Results obtained by using COE_{abcd} error definition; (b) results obtained by using COE_{ab} error definition. ◇, COE_{abcd} method results; ◆, COE_{ab} method results; ▬, simulated noise-free wave field parameters ($E'_{\mathrm{Est}}/E'_{\mathrm{Sim}} = 1$, $\eta = 0.06$).

Using these boundary conditions along with Eq. (2), also by noting $\hat{v} = \mathrm{i}\omega\hat{y}$, the wave coefficients can be calculated as

$$
\begin{aligned}
a &= \frac{1}{2}\frac{\mathrm{i}\omega\hat{F}_0\left[\mathrm{e}^{(1+\mathrm{i})kL} + \mathrm{e}^{2\mathrm{i}kL} + \mathrm{i}\mathrm{e}^{2(1+\mathrm{i})kL} + i\mathrm{e}^{(1+\mathrm{i})kL}\right]}{EIk^3\left[\mathrm{i}\mathrm{e}^{2kL} - \mathrm{i}\mathrm{e}^{2\mathrm{i}kL} - 1 + \mathrm{e}^{2(1+\mathrm{i})kL}\right]},\\
b &= \frac{1}{4}\frac{(-1+\mathrm{i})\omega\hat{F}_0\left[2\mathrm{e}^{(1+\mathrm{i})kL} + 1 - \mathrm{i}\mathrm{e}^{2kL} + \mathrm{e}^{2kL} + i\right]}{EIk^3\left[i\mathrm{e}^{2kL} - i\mathrm{e}^{2ikL} - 1 + \mathrm{e}^{2(1+i)kL}\right]},\\
c &= \frac{1}{2}\frac{\mathrm{i}\omega\hat{F}_0\left[\mathrm{e}^{2(1+\mathrm{i})kL} + \mathrm{i}\mathrm{e}^{2kL} + \mathrm{i}\mathrm{e}^{(1+\mathrm{i})kL} + \mathrm{e}^{(1+\mathrm{i})kL}\right]}{EIk^3\left[\mathrm{i}\mathrm{e}^{2kL} - \mathrm{i}\mathrm{e}^{2\mathrm{i}kL} - 1 + \mathrm{e}^{2(1+\mathrm{i})kL}\right]},\\
d &= -\frac{1}{2}\frac{\omega\hat{F}_0\left[-\mathrm{i}\mathrm{e}^{(1+\mathrm{i})kL} + \mathrm{e}^{2\mathrm{i}kL} - \mathrm{i} + \mathrm{e}^{(1+\mathrm{i})kL}\right]}{EIk^3\left[\mathrm{i}\mathrm{e}^{2kL} - \mathrm{i}\mathrm{e}^{2\mathrm{i}kL} - 1 + \mathrm{e}^{2(1+\mathrm{i})kL}\right]},
\end{aligned}
\tag{B2}
$$

where $\hat{F}_0$ is the excitation force in phasor form and L is the beam length.

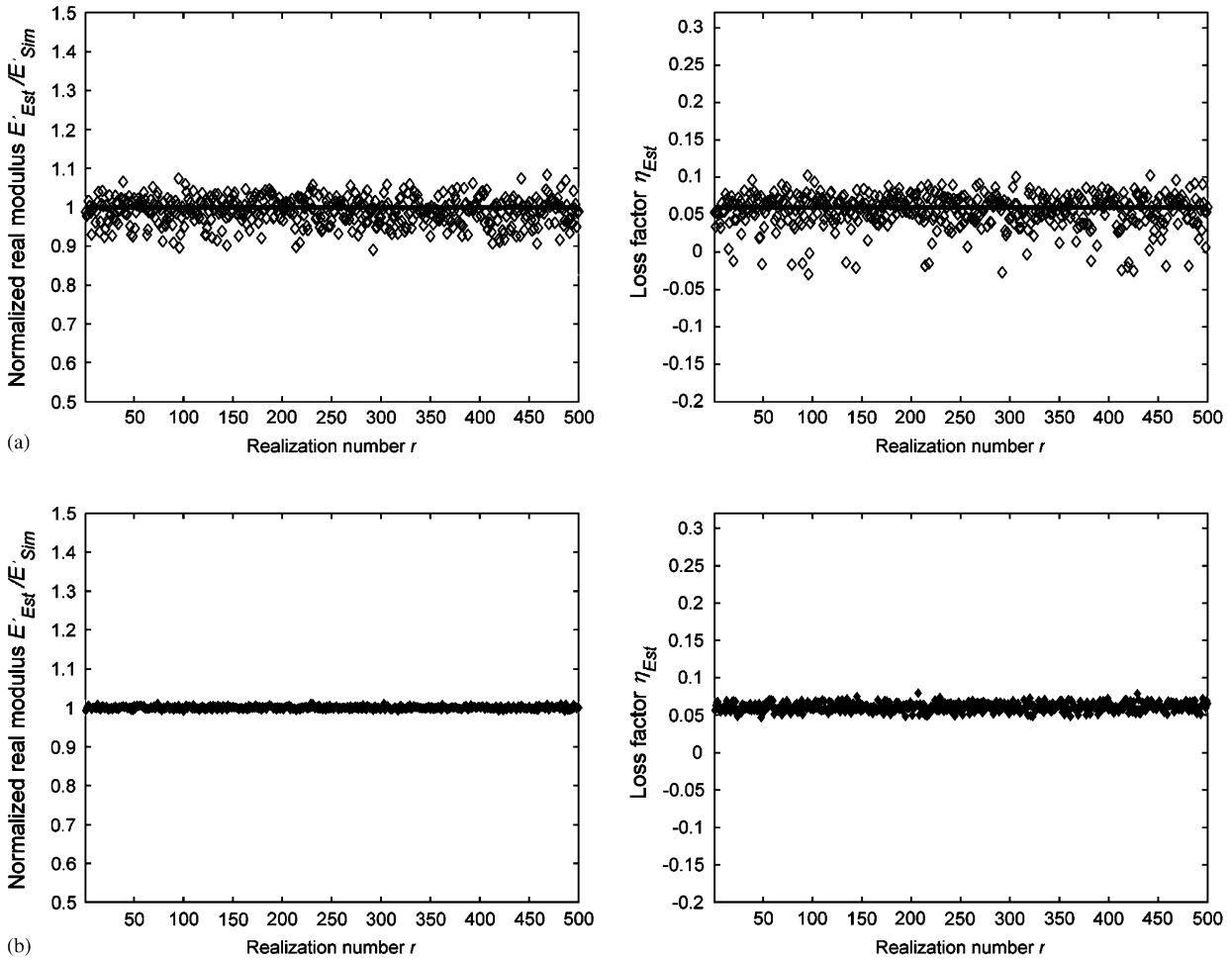

Fig. A2. Normalized real modulus $E'_{\mathrm{Est}}/E'_{\mathrm{Sim}}$ and loss factor η estimates vs. realization number r for error analysis with noise-free wave-field wavenumber $k = 27.4500 - \mathrm{i}0.4195$. (a) Results obtained by using COE_{abcd} error definition; (b) results obtained by using COE_{ab} error definition. ◇, COE_{abcd} method results; ◆, COE_{ab} method results; ▬, simulated noise-free wave field parameters ($E'_{\mathrm{Est}}/E'_{\mathrm{Sim}} = 1$, $\eta = 0.06$).

References

[1] R. Plunkett, *Measurement of Damping, Structure Damping*, ASME Publication, New York, 1959, pp. 117–131.
[2] L. Cremer, M. Heckl, E.E. Ungar, *Structure-Borne Sound*, second ed., 1988.
[3] D.I.G. Jones, *Handbook of Viscoelastic Vibration Damping*, Wiley, New York, 2001.
[4] G. Kurtze, K. Tamm, S. Vogel, Modellversuche Zur Biegewellendämmung an Ecken, *Acustica* 5 (1955) 223–233.
[5] H. Oberst, K. Frankenfeld, Uber die dampfung der biegeschwingungen dunner bleche durch fest haftendebelage, *Acustica* 2 (1952) 181–194.
[6] D. Ross, E.E. Ungar, E.M. Kerwin Jr., Damping of plate flexural vibrations by means of viscoelastic laminae, *Structural Damping*, ASME Publication, New York, 1959, pp. 49–88.
[7] A.J. Hull, D.A. Hurdis, A parameter estimation method for the flexural wave properties of a beam, *Journal of Sound and Vibration* 262 (2003) 187–197.
[8] L. Hillström, M. Mossberg, B. Lundberg, Identification of complex modulus from measured strains on an axially impacted bar using least squares, *Journal of Sound and Vibration* 230 (2000) 689–707.
[9] K. Mahata, S. Mousavi, T. Söderström, M. Mossberg, U. Valdek, L. Hillström, On the use of flexural wave propagation experiments for identification of complex modulus, *IEEE Transactions on Control Systems Technology* 11 (6) (2003) 863–874.
[10] L. Hillström, U. Valdek, B. Lundberg, Estimation of the state vector and identification of the complex modulus of a beam, *Journal of Sound and Vibration* 261 (2003) 653–673.

[11] S. Mousavi, D.F. Nicolas, B. Lundberg, Identification of complex moduli and Poisson's ratio from measured strains on an impacted bar, *Journal of Sound and Vibration* 277 (2004) 971–986.
[12] J.G. McDaniel, W.S. Shepard Jr., Estimation of structural wave numbers from spatially sparse response measurements, *Journal of the Acoustical Society of America* 108 (4) (2000) 1674–1682.
[13] MatWeb — Online Material Data Sheet, http://www.matweb.com.
[14] J. Koppelmann, *Rheologica Acta* 1 (1958) 20.
[15] J.D. Ferry, *Viscoelastic Properties of Polymers*, Wiley, New York, 1980.
[16] R.D. Blevins, *Formulas for Natural Frequency and Mode Shape*, Van Nostrand Reinhold, New York, 1979.